the COOH-terminus of the XIP3R protein (*8*). The mAbs to XIP3R were isolated by fusion of the P3U1 myeloma cell line P3x63AgU1 with spleen cells derived from BALB/c mice immunized with glutathione-S-transferase–XIP3R fusion protein. Initial screenings were done by enzyme-linked immunosorbent assays (ELISA) with TrpE-XIP3R fusion proteins. The serum-free culture supernatant of hybridoma cell lines and commercial mouse IgG used as controls were affinity purified with Ampure IgG purification kits (Amersham), followed by dialysis against injection buffer (88 mM NaCl, 1 mM KCl, 15 mM tris-HCl, pH 7.5). With the assumption that the volume of the 2-cell stage embryo is 1 μl [Y. Chen, L. Huang, M. Solursh, *Dev. Biol.* **161**, 70 (1994)], injection of antibody at 20 ng per embryo into the VMZs of 4-cell stage embryos resulted in the estimated final concentration of mAb of ~40 μg/ml.

10. S. Kume *et al*., *Dev. Biol.* **182**, 228 (1997).
11. The release of Ca^{2+} from microsomes of *Xenopus* oocytes by the addition of 100 nM IP_3 was measured. The amount of IICR was normalized to the amplitude of the Ca^{2+} release in the presence of control mouse IgG [A. Muto, S. Kume, T. Inoue, H. Okano, K. Mikoshiba, *J. Cell Biol.* **135**, 181 (1996)].
12. K. Fukuda *et al*., *Nature* **327**, 623 (1987).
13. The Ca^{2+} indicator dye Fura 2 (Molecular Probe) (20 μM) and m1AChR mRNA (13 ng per embryo) were micro-injected at the 2-cell stage, and then mAb (40 ng per embryo) was injected at the animal poles. Animal pole blastomeres were cut off between the 32- to 128-cell stage. Changes in the fluorescence intensities excited at 340 and 380 nm upon carbachol addition (100 μM) were recorded and analyzed.
14. P. D. Nieuwkoop and J. Faber, *The Normal Development Table of* Xenopus laevis (North-Holland, Amsterdam, 1967).
15. S. Kume, unpublished observation.
16. To obtain more precise information about the sequence that the inhibitory mAbs recognize, we synthesized a candidate epitope of a 12-residue-long peptide with the sequence GQPAHLNINPQQ (corresponding to residues 2680 to 2691, at the COOH terminal of XIP3R) (*8*) (Peptide Institute). Both ELISA and protein immunoblot analysis revealed that binding of the mAbs 11B12 and 1G9, but not 7F11, to XIP3R was inhibited in the presence of this peptide (*15*). Abbreviations for the amino acid residues are as follows: A, Ala; G, Gly; H, His; I, Ile; L, Leu; N, Asn; P, Pro; and Q, Gln.
17. Embryos were injected with 80 ng per embryo of 1G9 or control mouse IgG into the marginal zones of each blastomere at the 2-cell stage. DMZs or VMZs were explanted from stage 10 to 10.5 early gastrula embryos and cultured in 1× Steinberg's solution.
18. Total RNA was isolated from 10 explants. Reverse transcription was carried out with oligo(dT) primers. The primer pairs we used were described previously (*19*–*23*, *25*, *26*). RT-PCR products were stained with DNA-sensitive dye, SYBR Green I, and analyzed by FluorolImager (Molecular Dynamics).
19. Y. Sasai, *et al*., *Cell* **79**, 779 (1994); Y. Sasai, B. Lu, H. Steinbeisser, E. M. De Robertis, *Nature* **376**, 333 (1995).
20. A. Hemmati-Brivanlou, O. G. Kelly, D. A. Melton, *Cell* **77**, 283 (1994).
21. W. C. Smith and R. M. Harland, *ibid.* **70**, 829 (1992); W. C. Smith, A. K. Knecht, M. Wu, R. M. Harland, *Nature* **361**, 547 (1993).
22. F. Stutz and G. Spohr, *J. Mol. Biol.* **187**, 349 (1986).
23. K. W. Cho, B. Blumberg, H. Steinbeisser, E. M. De Robertis, *Cell* **67**, 1111 (1991).
24. G. Von Dassow, J. E. Schmidt, D. Kimelman, *Genes Dev.* **7**, 355 (1993).
25. V. Gawantka, H. Delius, K. Hirschfeld, C. Blumenstock, C. Niehrs, *EMBO J.* **14**, 6268 (1995).
26. C. R. Kintner and D. A. Melton, *Development* **99**, 311 (1987).
27. C. M. Jones, K. M. Lyons, P. M. Lapan, C. V. E. Wright, B. J. M. Hogan, *ibid.* **115**, 639 (1992); L. Dale, G. Howes, B. M. J. Price, J. C. Smith, *ibid*., p. 573.
28. S. Nishimatsu, A. Suzuki, A. Shoda, K. Murakami, N. Ueno, *Biochem. Biophys. Res. Commun.* **186**, 1487 (1992).
29. Our result that the expression of the ventral homeobox gene *Xvent-1*, a downstream component of BMP4 (*24*), was eliminated by 1G9 injection suggests that the expression of *Xvent-1* may be positively regulated by the IP_3-Ca^{2+} signaling system. Our present results show that the inhibition of the IP_3-Ca^{2+} signaling pathway induced the expression of *noggin* and *chordin* genes (Fig. 3). The up-regulation of these BMP4 antagonists by 1G9 injection suggests a negative regulation of these genes by the IP_3-Ca^{2+} signaling system, either directly or through negative cross-regulatory loops, as described between *Xvent-2* and *goosecoid* [D. Onichtchouk *et al*., *Development* **122**, 3045 (1996)]. As for the upstream factors that may activate the IP_3-Ca^{2+} signaling system, Xwnt-5A is a candidate [D. C. Slusarski, J. Yang-Snyder, W. B. Busa, R. T. Moon, *Dev. Biol.* **182**, 114 (1997)].
30. G. Thomsen *et al*., *Cell* **63**, 485 (1990); M. Asashima *et al*., *Roux's Arch. Dev. Biol.* **198**, 330 (1990); J. M. W. Slack, B. G. Darlington, J. K. Heath, S. F. Godsave, *Nature* **326**, 197 (1987); Y. Eto *et al*., *Biochem. Biophys. Res. Commun.* **142**, 1095 (1987).
31. J. C. Smith, B. M. Price, J. B. Green, D. Weigel, B. G. Herrmann, *Cell* **67**, 79 (1991).
32. J. C. Smith and J. M. Slack, *J. Embryol. Exp. Morphol.* **78**, 299 (1983); L. A. Lettice, J. M. W. Slack, *Development* **117**, 263 (1993).
33. P. Krieg, S. Varnum, M. Woormington, D. A. Melton, *Dev. Biol.* **133**, 93 (1989).
34. We thank M. Asashima and M. Yuge for invaluable advice, N. Ueno for the *Xenopus* BMP4 construct, S. Numa for the m1AchR construct, Y. Nishiuchi for synthesis of peptide, Y. Eto for purified human recombinant activin A. K. Okabe, Y. Takeyama, and H. Manki for technical assistance, T. Natsume for discussions, and N. Ueno, J. Aruga, and M. Ohara for critical comments on the manuscript. Supported by grants from the Ministry of Education, Science, Sports and Culture of Japan (H.O. and K.M.) and grants from research fellowships of the Japan Society for the Promotion of Science for Young Scientists (S.K.).

27 May 1997; accepted 9 October 1997

Crystal Structure of the Adenylyl Cyclase Activator $G_{s\alpha}$

Roger K. Sunahara, John J. G. Tesmer, Alfred G. Gilman, Stephen R. Sprang*

The crystal structure of $G_{s\alpha}$, the heterotrimeric G protein α subunit that stimulates adenylyl cyclase, was determined at 2.5 Å in a complex with guanosine 5′-*O*-(3-thiotriphosphate) (GTPγS). $G_{s\alpha}$ is the prototypic member of a family of GTP-binding proteins that regulate the activities of effectors in a hormone-dependent manner. Comparison of the structure of $G_{s\alpha}$·GTPγS with that of $G_{i\alpha}$·GTPγS suggests that their effector specificity is primarily dictated by the shape of the binding surface formed by the switch II helix and the α3-β5 loop, despite the high sequence homology of these elements. In contrast, sequence divergence explains the inability of regulators of G protein signaling to stimulate the GTPase activity of $G_{s\alpha}$. The βγ binding surface of $G_{s\alpha}$ is largely conserved in sequence and structure to that of $G_{i\alpha}$, whereas differences in the surface formed by the carboxyl-terminal helix and the α4-β6 loop may mediate receptor specificity.

The G_s and G_i subfamilies of heterotrimeric G protein α subunits, although highly homologous, differ profoundly with respect to effector, regulator, and receptor specificity (*1*, *2*). For example, $G_{s\alpha}$ binds to and activates all isoforms of adenylyl cyclase (*3*), whereas $G_{i\alpha 1}$ and its close paralogs inhibit only certain isoforms of the effector. The GTPase activities of G_i subfamily members are stimulated by members of the RGS (regulators of G protein signaling) protein family; the GTPase activity of $G_{s\alpha}$ is not affected by any known RGS protein (*4*). Distinct subfamilies of G protein–coupled receptors activate either G_s or G_i. To better understand the origins of these functional differences, we have determined the three-dimensional structure of GTPγS-activated $G_{s\alpha}$ alone and in complex with its effector, adenylyl cyclase (*5*). Comparison of the structure of $G_{s\alpha}$ with those of previously determined G_i subfamily members (*6*, *7*) offers substantial insight into the molecular basis of specificity in heterotrimeric G proteins.

Deficiencies in $G_{s\alpha}$ function have serious biological repercussions. Adenosine diphosphate (ADP) ribosylation of the active site residue Arg^{201} by cholera toxin (*8*, *9*) leads to irreversible inhibition of the GTPase activity of $G_{s\alpha}$. The resulting constitutive activation of adenylyl cyclase in gastrointestinal epithelium is responsible for the diarrhea and dehydration that are the hallmarks of cholera. Similarly, mutation of Arg^{201} or the catalytic residue Gln^{227} contributes to the growth of tumors of the pituitary and thyroid glands and causes the McCune-Albright syndrome (*10*, *11*). Heterozygous deficiency of $G_{s\alpha}$ is the basis for pseudohypoparathyroidism (type IA) (*11*–*13*).

R. K. Sunahara and A. G. Gilman, Department of Pharmacology, The University of Texas Southwestern Medical Center, 5323 Harry Hines Boulevard, Dallas, TX 75235–9041, USA.

J. J. G.Tesmer and S. R. Sprang, Howard Hughes Medical Institute and the Department of Biochemistry, University of Texas Southwestern Medical Center, 5323 Harry Hines Boulevard, Dallas, TX 75235–9050, USA.

*To whom correspondence should be addressed. E-mail: sprang@howie.swmed.edu

The structure of the active $G_{s\alpha}$·GTPγS complex was determined at 2.5 Å resolution by molecular replacement with the use of the atomic coordinates of $G_{i\alpha}$·GTPγS (*7*) as the search model (Table 1). The structure has been refined to conventional and free crystallographic *R* factors of 23 and 29%, respectively. Each asymmetric unit of the crystal contains a nonphysiological $G_{s\alpha}$ dimer oriented parallel to the *a* axis of the crystal. The dimer interface buries 2500 $Å^2$ of surface area and is additionally stabilized by 10 phosphate anions derived from the crystallization medium. These phosphates contribute an additional 900 $Å^2$ of buried surface area (Fig. 1A). Residues 1 through 33 and 392 through 394 (of 394 residues; the numbering is based on the long alternative splice variant) are disordered at the NH_2- and COOH-termini of the crystal structure. Residues 65 through 88 of subunit A and residues 70 through 86 of subunit B in linker 1 of the protein are also disordered.

$G_{s\alpha}$, like its homologs $G_{i\alpha}$ (*7*) and $G_{t\alpha}$ (*6*), consists of a Ras-like domain joined through two linker polypeptides to an α-helical domain that is unique to heterotrimeric G proteins (*2*). The structure of the α-helical domain of $G_{s\alpha}$, expressed as a recombinant protein, has been determined by nuclear magnetic resonance (NMR) (*14*) and is virtually identical to that of the corresponding domain in the intact subunit [root mean square deviation (rmsd) of 1.2 Å for 113 pairs of Cα atoms]. Both NMR and crystal structures demonstrate that the αB-αC loop is poorly ordered and that the proline at position 115 adopts the cis conformation. Relative to $G_{i\alpha}$ and $G_{t\alpha}$, $G_{s\alpha}$ contains three major polypeptide insertions (Fig. 1, B and C). The first of these (i1) is near the NH_2-terminus and is not visible in the $G_{s\alpha}$ structure. The second (i2) is incorporated into the linker 1 peptide (connecting α1 to αA). However, this insert is subject to alternative splicing; in the short splice variant of $G_{s\alpha}$ described here, linker 1 is only one residue longer than that in $G_{i\alpha}$. Unlike $G_{i\alpha}$, linker 1 in $G_{s\alpha}$ is partially disordered. The third (i3) is a 15-residue insertion between αG and α4 of the Ras-like domain. The i3 insertion folds into a flap that protrudes from the surface of the domain (Fig. 1B) and forms most of the noncrystallographic dimer interface. Conformational differences between the helical

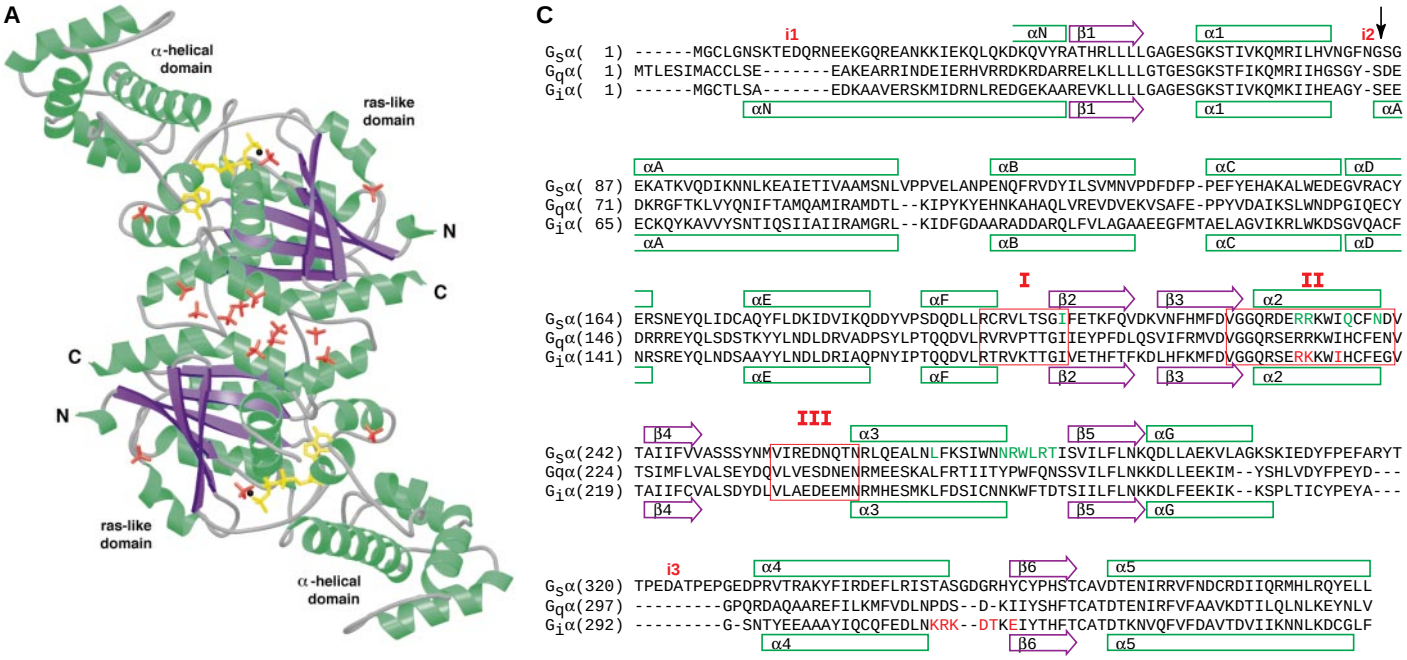

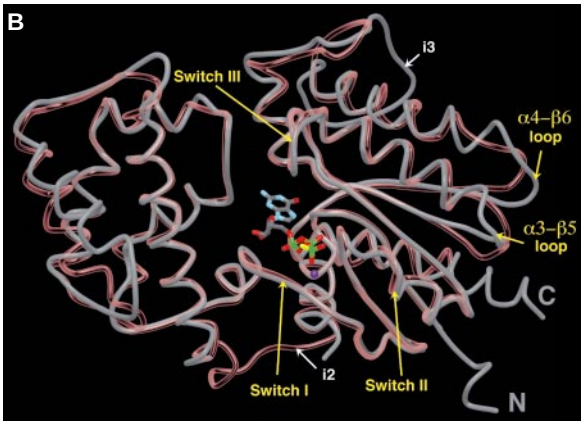

Fig. 1. The structure of $G_{s\alpha}$·GTPγS. (**A**) A dimer of $G_{s\alpha}$·GTPγS was observed in the asymmetric unit of the crystals and is depicted here as a ribbon and coil diagram looking down the noncrystallographic twofold axis. The 16 phosphate anions are drawn as red tetrahedrons. Most of the anions bind within a groove at the dimer interface between the α5 helices. The two phosphate anions that bind near the NH_2-termini of each molecule of $G_{s\alpha}$ form crystal contacts. GTPγS (yellow) and Mg^{2+} (black) are represented by ball-and-stick models and are located in the nucleotide binding pocket. Helices are green, β strands are purple, and coils are gray. This and the other ribbon diagrams were generated with MOLSCRIPT (*40*) and rendered with RASTER3D (*41*). (**B**) Superposition of $G_{i\alpha}$ (transparent rose) on the structure of $G_{s\alpha}$·GTPγS (solid gray). Only the nucleotide bound to $G_{s\alpha}$ is shown. The approximate locations of two of the three major insertions in the $G_{s\alpha}$ sequence relative to $G_{i\alpha}$ (i2 and i3) are indicated in white (see text). The two proteins superimpose with a rmsd of 1.0 Å for 260 Cα atom pairs. Their structures are essentially identical at the GTP binding site and are most divergent in various loops at the periphery of the molecule, most notably at the α3-β5 and α4-β6 loops. (**C**) Sequence alignment of representative proteins from three G_{α} subfamilies: bovine $G_{s\alpha}$ (Protein Information Resource accession number A23813), murine $G_{q\alpha}$ (A38414), and bovine $G_{i\alpha 1}$ (A23631) (*42*). Secondary structure has been assigned on the basis of the structures of $G_{s\alpha}$ and $G_{i\alpha 1}$·GTPγS (*7*). The three conformationally flexible switch elements are indicated by red blocks. The arrow marks the site in $G_{s\alpha}$ at which the long and short splice variants differ in length by 14 amino acids. Green amino acid letters indicate residues in $G_{s\alpha}$ that contact adenylyl cyclase, whereas red amino acid letters indicate potential adenylyl cyclase binding residues in $G_{i\alpha}$ identified by alanine-scanning mutagenesis (*21*). The general locations of the i1, i2, and i3 insertions are also indicated.

domains of $G_{s\alpha}$ and those of $G_{i\alpha}$ and $G_{t\alpha}$ have been noted previously (*7*, *14*). None of these differences involve regions of the subunit that participate in interactions with βγ (for $G_{i\alpha}$ and $G_{t\alpha}$) (*15*, *16*), RGS proteins (for $G_{i\alpha}$) (*17*), or adenylyl cyclase (for $G_{s\alpha}$) (*5*). In contrast, structural variations among these subunits in the α3-β5 and α4-β6 loops of the Ras-like domains (Fig. 2) are determinants of effector specificity (see below).

GTP is the organizing center for three switch elements (switches I through III) (Fig. 1, B and C) in G_α that undergo substantial conformational rearrangement upon GTP hydrolysis. These switch elements are also intimately involved in binding βγ, RGS family members, and effectors (*5*, *15*–*17*). The structure and orientation of all three switch elements are essentially identical in $G_{s\alpha}$·GTPγS, $G_{i\alpha}$·GTPγS (Fig. 1B), and $G_{t\alpha}$·GTPγS. The nucleotide is bound within the narrow cleft formed by switch I and switch II (Fig. 1, A and B), exactly as observed in the structures of the other G_α homologs. Indeed, the side chains that contact GTPγS and coordinate Mg^{2+} are identical to the corresponding residues in $G_{i\alpha}$. Electron densities corresponding to Mg^{2+}, one of its coordinating water molecules, and the presumptive hydrolytic water are observed. The second water ligand to Mg^{2+} is, however, evident in the $G_{s\alpha}$·adenylyl cyclase complex (*5*). Arg^{201}, which facilitates GTP hydrolysis by stabilizing the proposed pentavalent phosphate intermediate (*7*, *18*) and is the site of ADP ribosylation by cholera toxin (*8*, *9*), is exposed to solvent and partially ordered. Gln^{227}, which is conserved in most members of the Ras superfamily and is required for catalytic activity in heterotrimeric G proteins, forms no direct contacts with either the γ-thiophosphate of GTPγS or the presumptive hydrolytic water. This is also the case in the structures of other Ras superfamily members bound to GTP analogs (*2*).

Of all G_α homologs, only $G_{s\alpha}$ and G_{olf} activate adenylyl cyclase. It is evident from the structure of the complex between $G_{s\alpha}$ and the catalytic domains of adenylyl cyclase (*5*) that exclusion of $G_{i\alpha}$ from this site arises primarily from differences in the conformation, but not the amino acid composition, of the cyclase binding site. Residues that bind adenylyl cyclase are located in the α2 helix of switch II and the α3-β5 loop (*5*) (Figs. 1C and 3). Both segments were identified as potential adenylyl cyclase binding sites by alanine- and homolog-scanning mutagenesis (*19*, *20*). Of the nine $G_{s\alpha}$ side chains that directly interact with adenylyl cyclase, seven are invariant or highly conserved among the $G_{s\alpha}$ and $G_{i\alpha}$ proteins (Fig. 1C). The exceptions, Gln^{236} and Asn^{239}, are replaced by histidine and glutamic acid, respectively. The side chain of Asn^{239} stacks against the guanidinium group of Arg^{913} of type II adenylyl cyclase, and Gln^{236} serves as a hydrogen bond acceptor from Asn^{905}. The corresponding amino acid side chains in $G_{i\alpha}$ could potentially participate in analogous interactions. Indeed, mutation of these residues in $G_{s\alpha}$, along with Asp^{240}, to their counterparts in $G_{i\alpha}$, results in only a threefold reduction in the capacity to stimulate adenylyl cyclase activity (*20*). It is more likely that $G_{i\alpha}$ fails to activate adenylyl cyclase because its α3-β5 loop is displaced from the switch II helix, so that both elements cannot be simultaneously accommodated by the cyclase binding site. The relative shift is due to the substitution, in $G_{i\alpha}$, of a bulky phenylalanine residue for Leu^{282} in the helical α3-β5 loop (Fig. 2). To avoid collision with the conserved Phe^{215} ($G_{i\alpha}$) in switch II, α3-β5 is translated by approximately 1.5 Å. The α3-β5 loop of $G_{s\alpha}$ is also stabilized by a stacking interaction between Trp^{277} and His^{357} in the α4-β6 loop. No such stabilizing contacts are possible in $G_{i\alpha}$ because Trp^{277} and His^{357} are replaced by Cys^{264} and Lys^{317}, respectively, and because the α4-β6 loop of $G_{i\alpha}$ differs in sequence, length, and structure from the corresponding loop in $G_{s\alpha}$. Indeed, substitution of the $G_{i\alpha}$ α4-β6 loop into $G_{s\alpha}$ abolishes activation of adenylyl cyclase (*20*) by removing stabilizing interactions and perhaps also by disrupting adjacent effector binding regions. However, substitution of the $G_{s\alpha}$ α4-β6 sequence into $G_{i\alpha}$ fails to confer cyclase-stimulating activity because the α4-β6 loop supports, but does not form part of, the cyclase binding site. Switch II of $G_{i\alpha}$ and, less convincingly, its α4-β6 loop have been implicated in formation of the inhibitory complex with type V and VI adenylyl cyclases (*21*) at a site distinct from that rec-

Table 1. Summary of data collection and refinement statistics. The short-splice form of bovine $G_{s\alpha}$ was expressed with a COOH-terminal hexahistidine tag in *Escherichia coli* and purified to homogeneity on a nickel-nitrilotriacetic acid column, followed by hydroxyapatite and Mono Q fast protein liquid chromatography, essentially as described by Lee *et al*. (*32*). Purified $G_{s\alpha}$ was concentrated to 12 mg ml^{-1} (270 μM) and incubated with 800 μM GTPγS in a buffer containing 20 mM Na Hepes (pH 8.0), 5 mM $MgCl_2$, 1 mM EDTA, and 5 mM dithiothreitol (DTT). Crystals of $G_{s\alpha}$ were obtained at 20°C by hanging drop vapor diffusion. Hanging drops containing 6 μl total of a 1:1 mixture of activated $G_{s\alpha}$ and well solution were suspended over a 500-μl well containing 90 to 100% saturated KH_2PO_4 or 2.5 M NaH_2PO_4. The crystals, which form as bundles of 20-μm thick plates, belong to space group $P2_12_12_1$ and contain two molecules of $G_{s\alpha}$ per asymmetric unit. For data collection, individual crystals were harvested in a solution containing 2.5 M NaH_2PO_4, 25 mM sodium citrate (pH 4.5), 5 mM $MgSO_4$, 2 mM DTT, 1 mM EDTA, 150 μM GTPγS, and 15% glycerol as the cryoprotectant. The crystals were subsequently frozen in liquid propane and were maintained at −180°C during data collection. Diffraction data were collected from two crystals with the use of 0.908 Å radiation from the A1 beam line at the Cornell High-Energy Synchrotron Source (CHESS). The data were integrated and scaled with the HKL package (*33*), and the structure was solved by molecular replacement with the use of AMORE (*34*) as implemented by the CCP4 program suite (*35*). A cross-rotation function using $G_{i\alpha 1}$·GTP·γS (*7*) as the search model revealed only one significant peak. Subsequently, two translationally related molecules of $G_{s\alpha}$·GTPγS were located by the translation function. These two subunits constitute a noncrystallographic dimer oriented along the *a* axis of the unit cell. The initial atomic model was built by substituting $G_{i\alpha}$ side chains with their equivalents in $G_{s\alpha}$ using the program O (*36*), and subsequent manual model building was alternated with conventional and simulated annealing refinement in X-PLOR 3.851 (*37, 38*). The two molecules of $G_{s\alpha}$ were restrained by their noncrystallographic symmetry only for the first several rounds of refinement. The two subunits superimpose with a rmsd of 0.3 Å. The backbone conformations of 92% of the amino acids are within the most favored regions of the Ramachandran plot; there are no residues in disallowed regions (*39*). The model includes one molecule of Mg^{2+} and GTPγS per $G_{s\alpha}$ subunit and 16 phosphate anions. The average *B* factor is 26.5 $Å^2$.

Data collection statistics

Unit cell (Å)	Crystals (*n*)	D_{min} (Å)	Unique reflections	Average redundancy	R_{sym}* (%)	Completeness (%)	$\langle I \rangle / \langle \sigma_I \rangle$
a = 88.3 b = 96.5 c = 133.4	2	2.5	37,636	4.2	13.8	94	8.3

Refinement statistics

Protein atoms (*n*)	Water molecules (*n*)	Heterogen atoms (*n*)	Rmsd bond length (Å)	Rmsd bond angles (°)	Rmsd Δ*B* factor ($Å^2$)	R_{work}† (%)	R_{free}‡ (%)
5560	57	146	0.008	1.5	3.3	23	29

*$R_{sym} = \Sigma_h \Sigma_i |I(h) - I(h)_i| / \Sigma_h \Sigma_i I(h)_i$ where $I(h)$ is the mean intensity after rejections. †$R_{work} = \Sigma_h ||F_{obs}(h)| - |F_{calc}(h)|| / \Sigma h |F_{obs}(h)|$; includes all data from 15.0 to 2.5 Å and a bulk solvent correction. An I/σ cutoff was not used. ‡Ten percent of the complete data set was excluded from refinement to calculate R_{free}.

ognized by $G_{s\alpha}$ (*22*) (Fig. 1C). Switch III, which is stabilized by ionic contacts with switch II, does not contribute to the adenylyl cyclase binding site. Located at the NH_2-terminus of α3 distal to the α3-β5 loop, switch III adopts the same conformation in $G_{s\alpha}$ and $G_{i\alpha}$. Accordingly, disruption of an ionic contact between switch III and switch II through mutation of Arg^{231} only modestly reduces the stimulatory activity of $G_{s\alpha}$ (*23*).

$G_{s\alpha}$ does not undergo a conformational change upon binding to the soluble domains of adenylyl cyclase. The rmsd between the 334 Cα atom pairs in the free and bound forms of $G_{s\alpha}$ is 0.5 Å. The effector-binding regions of $G_{s\alpha}$, and perhaps those of other G_α subunits, are already maintained in a competent conformation in the GTPγS-bound form of the protein. In contrast, the switch II elements of both $G_{t\alpha}$ and $G_{i\alpha}$, and probably $G_{s\alpha}$, undergo substantial conformational changes when GDP is exchanged for GTPγS. Although the apparent affinity of adenylyl cyclase for $G_{s\alpha}$·GDP is only 10 times less than for $G_{s\alpha}$·GTPγS (*24*), $G_{s\alpha}$·GDP binds with much greater affinity to βγ subunits than does $G_{s\alpha}$·GTPγS (*25*). Consequently, full deactivation of adenylyl cyclase requires the rapid sequestration of $G_{s\alpha}$·GDP in a high-affinity complex with βγ.

Although the effector binding sites of $G_{s\alpha}$ and $G_{i\alpha}$ (or $G_{t\alpha}$) differ, the residues in the extensive βγ binding surfaces observed in $G_{i\alpha1}$ (Ile^{184}, Phe^{199}, Lys^{210}, Trp^{211}, Cys^{214}, and Phe^{215}) (*15*) are largely conserved in $G_{s\alpha}$. Superposition of the α subunits from both the $\alpha_i\beta_1\gamma_2$ heterotrimer and the $G_{s\alpha}$·adenylyl cyclase complex demonstrates that βγ and adenylyl cyclase bind to extensively overlapping sites on the α subunit (Fig. 3) and are similarly oriented with respect to the plasma membrane. Thus, βγ is a potent competitor with adenylyl cyclase for the GDP-bound form of $G_{s\alpha}$. Although the α3-β5 and α4-β6 loops have been implicated in effector binding and specificity, they do not participate in interactions with βγ (Fig. 3).

In contrast to the mechanism of effector recognition, the selectivity of RGS proteins for $G_{i\alpha}$ subunits (compared to $G_{s\alpha}$) can be attributed to differences in the amino acid composition rather than the conformation of the RGS binding site. The crystal structure of RGS4 complexed with $G_{i\alpha1}$·GDP·AlF_4^- demonstrates that RGS proteins activate GTP hydrolysis by binding to and stabilizing all three switch elements of $G_{i\alpha}$ in their transition state conformation (*17*). All RGS molecules characterized thus far are capable of accelerating the GTPase activities of $G_{i\alpha}$ or $G_{q\alpha}$ subfamily members (or both) but not of $G_{s\alpha}$ (*4*). Because the backbone conformations of the switch I and II elements are essentially identical in $G_{i\alpha}$ and $G_{s\alpha}$, the specificity of RGS for heterotrimeric G protein subfamilies is largely dictated by the identity of side chains within the switch elements. Six residues of $G_{i\alpha1}$ that come in contact with RGS4 are not conserved in $G_{s\alpha}$: Lys^{180} (Leu^{203} in $G_{s\alpha}$), Thr^{182} (Ser^{205}), and Val^{185} (Phe^{208}) in switch I; and Ser^{206} (Asp^{229}), Lys^{209} (Arg^{232}), and His^{213} (Gln^{236}) in switch II. These substitutions deter binding of RGS proteins to $G_{s\alpha}$ by steric overlap, charge repulsion, or the creation of small cavities in the interface (for example, the substitution of Thr^{182} by Ser^{205}). Although each substitution alone does not seem sufficient to disrupt a potential RGS·$G_{s\alpha}$ complex, their cumulative effects apparently are.

Surprisingly, the "footprint" of RGS4, as mapped onto the surface of $G_{s\alpha}$, does not substantially overlap with that of adenylyl cyclase (Fig. 3). Superposition of $G_{i\alpha1}$·RGS4 on $G_{s\alpha}$·adenylyl cyclase reveals only minor potential steric conflicts between adenylyl cyclase and RGS4, although no substantial interface exists between them. Assuming an analogous interaction between switch II of $G_{i\alpha}$ and as-yet-unidentified domains of type V and VI adenylyl cyclase, RGS4 could potentially accelerate GTP hydrolysis while $G_{i\alpha}$ is still bound to adenylyl cyclase. This in turn suggests the possibility that RGS proteins and adenylyl cyclase, perhaps along with heterotrimeric G proteins and their receptors, exist as discrete complexes on the membrane of the cell after activation of G protein–coupled receptors.

The fidelity of signal transduction depends on the capacity of G protein–coupled receptors to distinguish among the unique structural features of various G_α subunits. Although the surface contacted by the receptor probably includes segments of the β subunit and the NH_2-terminus of G_α, the COOH-terminus of G_α contributes importantly to receptor selectivity [reviewed in (*26*)]. Evidence gained from alanine-scanning mutagenesis (*27*) and patterns of evolutionary conservation (*28*) also argue for inclusion of the α4-β6 loop and the α5 helix in the receptor binding surface. The α5 helix of $G_{s\alpha}$ is kinked at its midsection and bends around the underlying β sheet

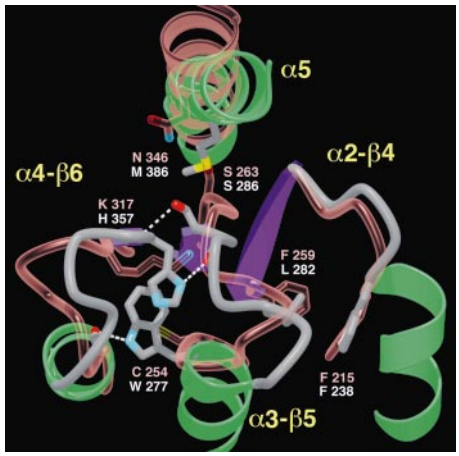

Fig. 2. Superposition of the putative effector binding loops (α2-β4, α3-β5, and α4-β6) and the α5 helix from $G_{s\alpha}$ onto $G_{i\alpha}$ (*42*). The side chains from residues of $G_{s\alpha}$ are drawn as stick models with the use of conventional coloring. The backbone and side chains of $G_{i\alpha}$ are illustrated in transparent rose. The model of $G_{i\alpha}$ is derived from the structure of the $G_{i\alpha1}$·RGS4 complex (*17*), which has a completely ordered α5 helix. The superposition is essentially the same as that shown in Fig. 1B. The α2-β4 loops of each α subunit are essentially identical. The α3-β5 loop of $G_{s\alpha}$, although structurally similar to that of $G_{i\alpha}$, is rotated downward in the figure. This rotation creates a hydrophobic pocket on the back side of the β sheet, which is filled by the side chain of Met^{386} from the α5 helix, and moves the residue at position 282 in $G_{s\alpha}$ toward the conserved Phe^{238}. In the G_s subfamily, residue 282 is a leucine, which helps to accommodate the shift of the α3-β5 loop. The α4-β6 loop of $G_{s\alpha}$ is longer than and shares no sequence identity with its counterpart in $G_{i\alpha}$. The α3-β5 and α4-β6 loops are supported by a stacking interaction between Trp^{277} and His^{357}, both of which are invariant in the G_s subfamily. The α5 helix of $G_{s\alpha}$ is bent, whereas that of $G_{i\alpha}$ extends straight into solvent. The large differences observed in the α4-β6 and α5 structures may help account for receptor specificity among closely related α subunits.

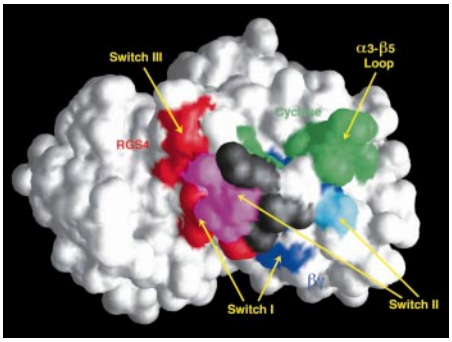

Fig. 3. Interaction footprints of G_α regulators and effectors. Surfaces representing contact regions of βγ (blue), RGS4 (red), and adenylyl cyclase (green) are mapped onto the solvent-accessible surface of $G_{s\alpha}$ (*43*). A contact was defined as an interatomic distance of less than 4.0 Å. Residues that contact both adenylyl cyclase and βγ are colored cyan, those that contact both RGS4 and βγ are magenta, and those that interact with all three are dark gray. RGS4 and adenylyl cyclase have few if any significant steric overlaps; the gray areas thus represent cases where each protein contacts a different part of the same G_α residue. The figure was generated with GRASP (*43*).

(Figs. 1A and 2). The α4-β6 loop is in close proximity to the COOH-terminus of α5. The contact is stabilized by insertion of Met^{386} into a hydrophobic pocket formed by the NH_2-terminal residues of β5 and β6. Together, the α4-β6 loop and the α5 helix form a plane on the back side of $G_{s\alpha}$ that may interact with receptors (*29*–*31*). In contrast, the corresponding α5 helix in $G_{i\alpha}$ (as visualized in the structures of the $G_{i\alpha 1}$·GDP·$\beta_1\gamma_2$ and $G_{i\alpha 1}$·GDP·AlF_4^-·RGS4 complexes) is relatively straight and extends away from the central β sheet of the Ras-like domain (Fig. 2). The relative position of the α4-β6 loop of $G_{s\alpha}$ also differs from that of the cognate loop of $G_{i\alpha}$. The divergence of these two structural elements from those of $G_{i\alpha}$ and $G_{t\alpha}$ may therefore contribute to receptor selectivity.

REFERENCES AND NOTES

1. E. J. Neer, *Cell* **80**, 249 (1995).
2. S. R. Sprang, *Annu. Rev. Biochem*. **66**, 639 (1997).
3. R. K. Sunahara, C. W. Dessauer, A. G. Gilman, *Annu. Rev. Pharmacol. Toxicol*. **36**, 461 (1996).
4. D. M. Berman and A. G. Gilman, *J. Biol. Chem*., in press.
5. J. J. G. Tesmer, R. K. Sunahara, A. G. Gilman, S. R. Sprang, *Science* **278**, 1907 (1997).
6. J. P. Noel, H. E. Hamm, P. B. Sigler, *Nature* **366**, 654 (1993).
7. D. E. Coleman *et al.*, *Science* **265**, 1405 (1994).
8. D. Cassel and Z. Selinger, *Proc. Natl. Acad. Sci. U.S.A.* **74**, 3307 (1977).
9. C. Van Dop, M. Tsubokawa, H. R. Bourne, J. Ramachandran, *J. Biol. Chem*. **259**, 696 (1984).
10. J. Lyons *et al.*, *Science* **249**, 655 (1990).
11. A. M. Spiegel, *Annu. Rev. Physiol.* **58**, 143 (1996).
12. T. Iiri, P. Herzmark, J. M. Nakamoto, C. Van Dop, H. R. Bourne, *Nature* **371**, 164 (1994).
13. Z. Farfel *et al.*, *J. Biol. Chem*. **271**, 19653 (1996).
14. D. R. Benjamin, D. W. Markby, H. R. Bourne, I. D. Kuntz, *J. Mol. Biol*. **254**, 681 (1995).
15. M. A. Wall *et al.*, *Cell* **80**, 1047 (1995).
16. D. G. Lambright *et al.*, *Nature* **379**, 311 (1996).
17. J. J. G. Tesmer, D. M. Berman, A. G. Gilman, S. R. Sprang, *Cell* **89**, 251 (1997).
18. J. Sondek, D. G. Lambright, J. P. Noel, H. E. Hamm, P. B. Sigler, *Nature* **372**, 276 (1994).
19. H. Itoh and A. G. Gilman, *J. Biol. Chem*. **266**, 16226 (1991).
20. C. H. Berlot and H. R. Bourne, *Cell* **68**, 911 (1992).
21. G. Grishina and C. H. Berlot, *J. Biol. Chem*. **272**, 20619 (1997).
22. R. Taussig, W.-J. Tang, J. R. Hepler, A. G. Gilman, *ibid.* **269**, 6093 (1994).
23. T. Iiri, Z. Farfel, H. R. Bourne, *Proc. Natl. Acad. Sci. U.S.A.* **94**, 5656 (1997).
24. C. W. Dessauer, T. T. Scully, A. G. Gilman, *J. Biol. Chem*. **272**, 22272 (1997).
25. A. G. Gilman, *Annu. Rev. Biochem*. **56**, 615 (1987).
26. H. R. Bourne, *Curr. Opin. Struct. Biol*. **9**, 134 (1997).
27. R. Onrust *et al.*, *Science* **275**, 381 (1997).
28. O. Lichtarge, H. R. Bourne, F. E. Cohen, *Proc. Natl. Acad. Sci. U.S.A.* **93**, 7507 (1996).
29. B. R. Conklin and H. R. Bourne, *Cell* **73**, 631 (1993).
30. S. B. Masters *et al.*, *Science* **241**, 448 (1988).
31. M. M. Rasenick, M. Watanabe, M. B. Lazarevic, S. Hatta, H. E. Hamm, *J. Biol. Chem*. **269**, 21519 (1994).
32. E. Lee, M. E. Linder, A. G. Gilman, *Methods Enzymol*. **237**, 146 (1994).
33. Z. Otwinowski, in *Data Collection and Processing*, N. I. L. Sawyer and S. W. Bailey, Eds. (Science and Engineering Council, Daresbury Laboratory, Daresbury, UK, 1993), pp. 56–62.
34. J. Navaza, *Acta Crystallogr*. **A50**, 157 (1994).
35. S. Bailey, *ibid.* **D50**, 760 (1994).
36. T. A. Jones, J.-Y. Zou, S. W. Cowan, *ibid.* **A47**, 110 (1991).
37. A. T. Brünger, A. Krukowski, J. W. Erickson, *ibid.* **A46**, 585 (1990).
38. A. T. Brünger, X-PLOR Version 3.1 (Yale Univ. Press, New Haven, CT, 1992).
39. R. A. Laskowski, M. W. MacArthur, D. S. Moss, J. M. Thornton, *J. Appl. Crystallogr*. **26**, 283 (1993).
40. P. J. Kraulis, *ibid.* **24**, 946 (1991).
41. E. A. Merritt and M. E. P. Murphy, *Acta Crystallogr*. **D50**, 869 (1994).
42. Single-letter abbreviations for the amino acid residues are as follows: A, Ala; C, Cys; D, Asp; E, Glu; F, Phe; G, Gly; H, His; I, Ile; K, Lys; L, Leu; M, Met; N, Asn; P, Pro; Q, Gln; R, Arg; S, Ser; T, Thr; V, Val; W, Trp; and Y, Tyr.
43. A. Nicholls, K. A. Sharp, B. Honig, *Proteins* **11**, 281 (1991).

44. We thank J. Collins for superb technical assistance; C. Kleuss (Frie University, Berlin) for supplying $G_{s\alpha}$-H6 cDNA; B. Posner and D. Coleman for helpful discussion; D. Coleman, T. Harrell, T. Xiao, and the MacCHESS staff for their assistance with data collection at CHESS; and L. Esser for his assistance in preparing figures. R.K.S. was supported by a postdoctoral fellowship from the Medical Research Council of Canada. This work was supported by NIH grant DK46371 and Welch Foundation grant I-1229 to S.R.S. and by NIH grant GM34497, American Cancer Society grant RPG-77–001–21-BE, Welch Foundation grant I-1271, and the Raymond and Ellen Willie Distinguished Chair of Molecular Neuropharmacology to A.G.G. Atomic coordinates have been deposited with the Protein Data Bank (1AZT).

24 October 1997; accepted 14 November 1997

Mediation of Sonic Hedgehog–Induced Expression of COUP-TFII by a Protein Phosphatase

Venkatesh Krishnan, Fred A. Pereira, Yuhong Qiu, Chien-Huan Chen, Philip A. Beachy, Sophia Y. Tsai,* Ming-Jer Tsai*†

A Sonic hedgehog (Shh) response element was identified in the chicken ovalbumin upstream promoter–transcription factor II (COUP-TFII) promoter that binds to a factor distinct from *Gli*, a gene known to mediate Shh signaling. Although this binding activity is specifically stimulated by Shh-N (amino-terminal signaling domain), it can also be unmasked with protein phosphatase treatment in the mouse cell line P19, and induction by Shh-N can be blocked by phosphatase inhibitors. Thus, Shh-N signaling may result in dephosphorylation of a target factor that is required for activation of COUP-TFII–, Islet1-, and Gli response element–dependent gene expression. This finding identifies another step in the Shh-N signaling pathway.

COUP-TFs belong to the orphan receptor subfamily within the steroid–thyroid hormone receptor superfamily and are found in all vertebrate species examined (*1*). In the mouse there are two COUP-TF members, COUP-TFI and COUP-TFII. Both are expressed in the neural tube during embryonic development; however, COUP-TFII is highly expressed and displays a restricted expression pattern that is coincident with motor neuron differentiation (*1*). Transplantation of a notochord to the dorsal side of the chick neural tube results in ectopic expression of COUP-TFII that coincides with the appearance of motor neuron markers such as Isl1 and SC-1 in these regions (*2*).

V. Krishnan, F. A. Pereira, Y. Qiu, S. Y. Tsai, M.-J. Tsai, Department of Cell Biology, Baylor College of Medicine, 1 Baylor Plaza, Houston, TX 77030 USA.
C.-H. Chen and P. A. Beachy, Department of Molecular Biology and Genetics, Howard Hughes Medical Institute, Johns Hopkins University, School of Medicine, Baltimore, MD 21205 USA.

*These authors contributed equally to this report.
†To whom correspondence should be addressed. E-mail: mtsai@bcm.tmc.edu

Sonic hedgehog (*Shh*) is a vertebrate homolog of the *Drosophila* segment polarity gene hedgehog (*Hh*) (*3*). The secreted Shh protein (Shh-N) from the notochord is required for induction of floor plate cells, motor neurons, and other axial midline structures (*4*–*7*). To investigate whether Shh activates COUP-TFII expression, we asked whether purified recombinant Shh-N expressed in *Escherichia coli* can induce COUP-TFII expression in P19 cells (*8*). Increased COUP-TFII expression is observed at Shh-N concentrations as low as 0.2 nM (Fig. 1A, lane 2). This concentration is similar to the amount that is required for regulating other Shh-N target genes (*3*, *9*) and for binding to its putative receptor, patched (*ptc*) (*10*, *11*).

To identify the target element or elements for Shh-N signaling, we used deletion analysis and identified a sequence between −1316 and −1298 nucleotides in the COUP-TFII promoter that increases reporter gene activity when linked to a heterologous herpes simplex virus thymidine kinase (*tk*) promoter (*12*) (Fig. 2). Point